ADVANCED MATERIALS
www.advmat.de

# A Silica-Aerogel-Reinforced Composite Polymer Electrolyte with High Ionic Conductivity and High Modulus

*Dingchang Lin, Pak Yan Yuen, Yayuan Liu, Wei Liu, Nian Liu, Reinhold H. Dauskardt,* and Yi Cui**

**High-energy all-solid-state lithium (Li) batteries have great potential as next-generation energy-storage devices. Among all choices of electrolytes, polymer-based systems have attracted widespread attention due to their low density, low cost, and excellent processability. However, they are generally mechanically too weak to effectively suppress Li dendrites and have lower ionic conductivity for reasonable kinetics at ambient temperature. Herein, an ultrastrong reinforced composite polymer electrolyte (CPE) is successfully designed and fabricated by introducing a stiff mesoporous $SiO_2$ aerogel as the backbone for a polymer-based electrolyte. The interconnected $SiO_2$ aerogel not only performs as a strong backbone strengthening the whole composite, but also offers large and continuous surfaces for strong anion adsorption, which produces a highly conductive pathway across the composite. As a consequence, a high modulus of ≈0.43 GPa and high ionic conductivity of ≈0.6 mS $cm^{-1}$ at 30 °C are simultaneously achieved. Furthermore, $LiFePO_4$–Li full cells with good cyclability and rate capability at ambient temperature are obtained. Full cells with cathode capacity up to 2.1 mAh $cm^{-2}$ are also demonstrated. The aerogel-reinforced CPE represents a new design principle for solid-state electrolytes and offers opportunities for future all-solid-state Li batteries.**

High-energy and safe lithium (Li) batteries are in ever-growing demand as the power sources in electronics and electric vehicles.[1–3] Nevertheless, the state-of-the-art Li-ion cells encounter bottlenecks to further boost energy density, which calls for innovations in new battery chemistries beyond Li ion. Li metal has recently garnered intense interest as an anode candidate as it has the highest theoretical capacity of all alternatives (3860 mAh $g^{-1}$) and the lowest electrochemical potential (−3.04 V vs standard hydrogen electrode), promising an approximately twofold to fivefold higher specific density when combined with high capacity cathodes.[3–7] However, Li anodes are prone to metallic Li dendrite growth during battery cycling which can propagate through separators and internally short the two electrodes.[3,4,8] The resulting intense exothermic reaction can quickly heat up the cells and cause thermal runaway. These safety hazards are one of the major hurdles to commercialization. In liquid electrolyte systems, a promising strategy is to incorporate a mechanically strong separation layer such as anodized aluminum oxide with liquid electrolyte.[9,10] However, problems of high flammability of the liquid electrolytes and side reactions with metallic Li still remain.[11]

Transition to all-solid-state battery systems holds great promise in solving the above challenges. First, employing a high-modulus solid electrolyte provides a mechanical obstacle which can effectively hinder Li dendrite formation and penetration, circumventing internal short circuits. Second, replacing highly flammable liquid electrolytes would significantly diminish the possible explosion hazards. Moreover, the removal of liquid electrolytes may reduce the side reactions and suppress the shuttling of the cathode species to anode.

Solid electrolytes fall into two main categories, namely, inorganic ceramic electrolytes and solid polymer electrolytes (SPEs). The former term includes all the inorganic Li-ion conductors such as sulfides,[12–14] oxides,[15–17] nitrides,[18] and phosphates,[19,20] while the latter describes the Li salt/polymer blends.[21–25] In general, the inorganic ceramics afford high Li-ion conductivity close to or even surpassing that of their liquid counterparts, while their elastic modulus is also sufficiently high.[14,26] However, a high elastic modulus by itself is not necessary to fully suppress Li dendrites and internal short circuits. The formation of cracks, the diffusion of Li through grain boundaries, and oriented porosity may facilitate dendritic growth and internal short circuits.[27] In addition, several factors currently prohibit their practical application. First, the high density of inorganic ceramics compared to liquids severely

Dr. D. Lin, Y. Liu, Dr. W. Liu, Dr. N. Liu, Prof. R. H. Dauskardt, Prof. Y. Cui
Department of Materials Science and Engineering
Stanford University
Stanford, CA 94305, USA
E-mail: dauskardt@stanford.edu; yicui@stanford.edu
Dr. P. Y. Yuen
Department of Mechanical Engineering
Stanford University
Stanford, CA 94305, USA
Prof. Y. Cui
Stanford Institute for Materials and Energy Sciences
SLAC National Accelerator Laboratory
2575 Sand Hill Road, Menlo Park, CA 94025, USA
The ORCID identification number(s) for the author(s) of this article can be found under https://doi.org/10.1002/adma.201802661.

DOI: 10.1002/adma.201802661

 

decreases the specific energy of the cells, and second, the electrochemical stability windows of many inorganic ceramics are narrow, resulting in side reactions at the interfaces with the electrodes.[28] Finally, limitations of traditional ceramic fabrication make it challenging to produce thin- and large-area ceramic electrolytes that meet commercial standards.

SPEs have significant processing advantages, but are generally mechanically too weak and compliant to effectively suppress Li dendrite formation. Also, their Li-ion conductivity is mediocre, at least 2–3 orders of magnitude lower than liquids, limiting the delivery of sufficient power at ambient temperature.[24,29,30]

Multiple approaches have been employed to address these SPE's limitations. One is to add inorganic fillers into SPEs to enhance ionic conductivity.[21,23] However, the fillers are prone to agglomeration which reduces their efficacy for Lewis acid–base interaction and the resulting ionic conductivity is insufficient for battery kinetics. In addition, the fillers fail to form an interconnected reinforcement to effectively enhance the mechanical properties of the composites. Both ionic conductivity and mechanical properties are insufficient to satisfy commercial requirements. Another approach is to introduce plasticizers into Li salt/polymer blends to significantly boost ionic conductivity to practical values, but this is achieved at the expense of even further reduced mechanical properties and increased flammability.[31–33] A third recent approach is to blend polymer electrolytes with inorganic ion conductors,[34,35] though with success in demonstrating further improved ionic conductivity, the mechanical requirements are yet to be met.

In fact, there is an ionic conductivity versus elastic modulus dilemma in SPEs. High ionic conductivity generally requires low crystallinity and more mobile polymer chains, which in turn leads to mechanically softer polymers. To achieve viable SPEs that can suppress Li dendrites and deliver high power, this dilemma must be circumvented.

Herein, a $SiO_2$-aerogel-reinforced composite polymer electrolyte (CPE) has been developed to resolve the dilemma. In this design, the unique properties of the aerogel, which exhibits high elastic modulus, high porosity and, notably, a large internal surface area, all play key roles. By incorporating the strong $SiO_2$ aerogel backbone, the mechanical properties of the composite electrolytes are markedly improved, allowing the electrolyte to mechanically suppress the growth of Li dendrites. The high porosity further facilitates a large-volume occupancy of polymer electrolyte within the composite, enabling more efficient Li-ion conduction. Finally, the ultrafine and well-distributed $SiO_2$ domains with their large internal surface area promote more pronounced Lewis acid–base interaction with anions and thus enable higher dissociation of Li salts. The interconnected $SiO_2$ aerogel network with continuous regions of high anion adsorption further boosts ionic conductivity.

With the above merits, a $SiO_2$-aerogel-reinforced CPE with a high modulus of ≈0.43 GPa, nearly 2 orders of magnitude higher than that of conventional polymer electrolytes, and a high ambient temperature ionic conductivity of ≈0.6 mS $cm^{-1}$ at 30 °C was achieved. The $SiO_2$-aerogel-reinforced CPE effectively suppressed Li dendrites, allowing a prolonged cycle life without short circuit. Owing to its high ionic conductivity, ambient condition operation of the $LiFePO_4$ (LFP)–Li full cell with good cyclability and rate capability was obtained, full cells with high areal capacity up to 2.1 mAh $cm^{-2}$ are demonstrated. The new design offers a promising methodology solving the ionic conductivity versus modulus dilemma in SPEs and paves the way for the future advanced Li batteries.

The major synthetic procedures of the $SiO_2$-aerogel-reinforced CPEs are schematically shown in **Figure 1**a. With the $SiO_2$ aerogel as the starting framework, an electrolyte precursor composed of 6:4:8 (in weight) poly(ethylene glycol) diacrylate (PEGDA, $M_v \approx 700$, with 1 wt% CIBA IRGACURE 819):succinonitrile (SCN):lithium bis(trifluoromethanesulfonyl)imide (LiTFSI) was infused into the aerogel under vacuum, followed by photocuring to form crosslinked poly(ethylene oxide) (PEO) under 365 nm ultraviolet light (Figure S1, Supporting Information). The as-obtained composite, as illustrated in the magnified scheme in the right of Figure 1a, is a 3D continuous $SiO_2$ network embedded in the bulk of the crosslinked-PEO electrolyte. The $SiO_2$ aerogel network is distinct from separator designs in liquid electrolyte systems because it is designed to be filled with solid polymer electrolytes.[9,10] The transition to solid polymer systems imposes much more exacting requirements on the mechanical reinforcement, including porosity, microstructure, and surface chemistry of the $SiO_2$ aerogel, as discussed in the following sections. Notably, due to the light weight of the $SiO_2$ aerogel, the crosslinked-PEO electrolyte forms the majority of the composite, while the aerogel and the residual LiF only makes up ≈22 wt% (Figures S2 and S3, Supporting Information). This guarantees a large volume ratio of the ionically conductive phase that would not compromise ionic conductivity, which is critical for SPE systems. Figure 1b shows the pristine as-synthesized $SiO_2$ aerogel prior to precursor infusion, which exhibited a typical translucent nature and blue color due to Rayleigh scattering by the nanosized pores. The $SiO_2$-aerogel-reinforced CPE in Figure 1c, however, exhibits high clarity due to the full occupancy of the pores, which significantly reduces the scattering effect by improved matching of the refractive index of the $SiO_2$ and the polymer electrolyte. Scanning electron microscopy (SEM) images (Figure 1d,e and Figure S4 (Supporting Information)) show the pristine aerogel exhibiting a well-distributed and high density of small pores (Figure 1d) that were later filled by the polymer electrolyte (Figure 1e). In addition, the thickness of the $SiO_2$ aerogel film can be controlled during the alcogel formation step to be as thin as 30 μm (Figure S5, Supporting Information), which adds more fabrication flexibility to the electrolyte.

The surface area and size distribution of the pores were also determined by $N_2$ adsorption–desorption analysis. The results show that the $SiO_2$ aerogel affords a high Brunauer–Emmett–Teller (BET) surface area of 701 $m^2$ $g^{-1}$, comparable to those reported elsewhere.[36] In addition, a relatively narrow pore size distribution with the majority falling in the mesoporous regime was obtained.

The surface chemistry of the $SiO_2$ aerogel was characterized by Fourier transform infrared spectroscopy (FTIR) (Figure S6, Supporting Information). The FTIR spectrum clearly showed acidic hydroxyl (−OH) groups on the aerogel surface. These hydroxyl groups were produced during the cold $CO_2$ supercritical drying process in the aerogel fabrication process, and were shown to exhibit a coverage of ≈4–6 −OH $nm^{-2}$.[37] The acidic surface of the $SiO_2$ aerogel, the high surface area and uniformly

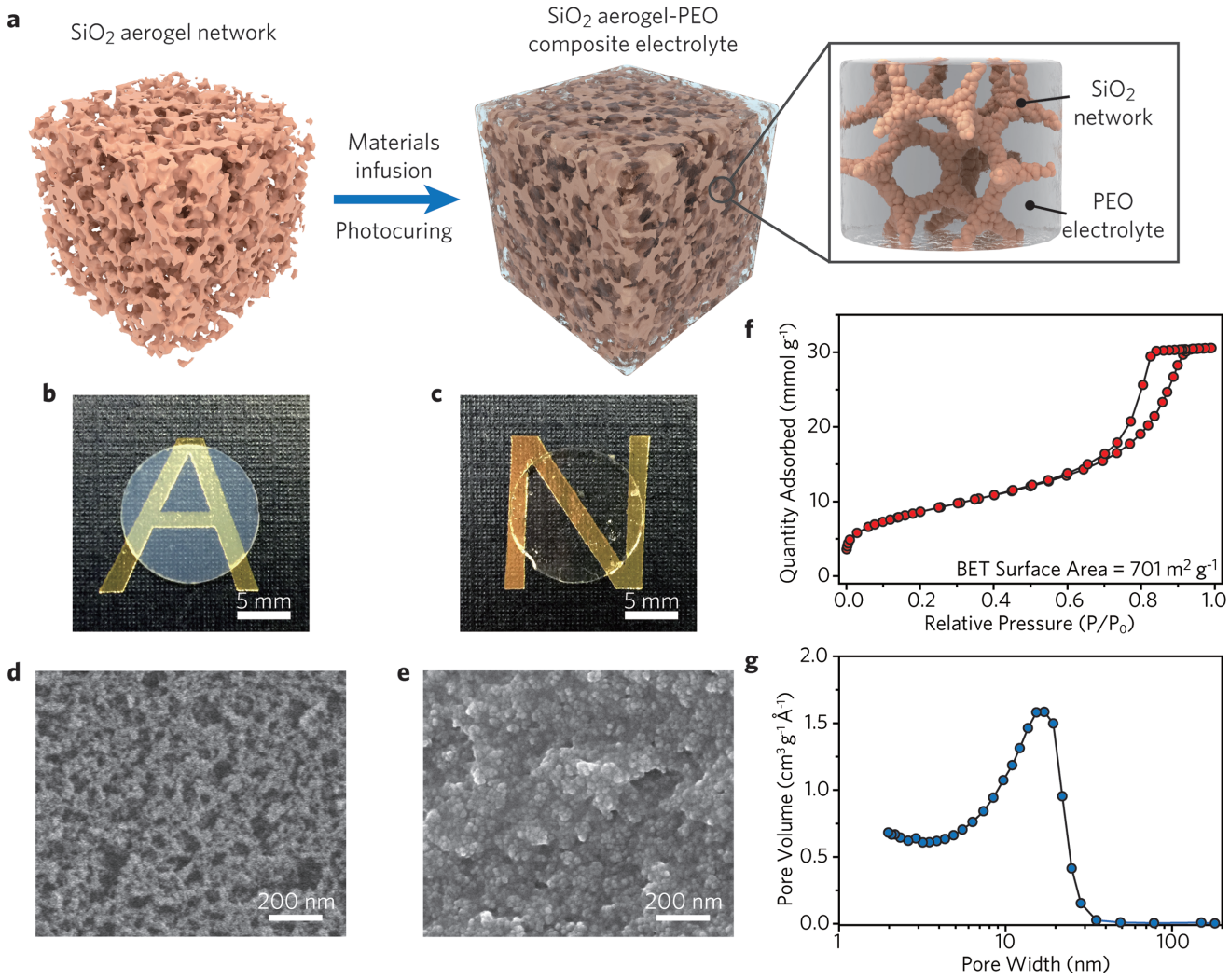


**Figure 1.** Material synthesis and characterizations. a) Schematic showing the synthetic procedures of the $SiO_2$-aerogel-reinforced CPE. With the $SiO_2$ aerogel as the framework, LiTFSI dissolved in liquid PEGDA/SCN mixture was infused into the aerogel under vacuum, followed by ultraviolet photocuring to afford crosslinked PEO within the aerogel framework. The magnified drawing in the right shows the detailed microstructure of the composite electrolyte. b,c) Digital photo images showing the pristine $SiO_2$ aerogel film (b) and the final composite electrolyte film (c), where the infusion of the materials increases the transparency of the film. d,e) SEM images showing the surface morphologies of pristine $SiO_2$ aerogel (d) and composite electrolyte (e). The high-volume pores are fully filled after infusion and photocuring. f,g) BET surface area (f) and pore size distribution (g) of the $SiO_2$ aerogel, which exhibits high surface area of 701 $m^2$ $g^{-1}$ with most of the pores <30 nm.

distributed pores facilitate Lewis acid–base interaction for anion adsorption,[21] which plays a key role in SPE systems for favorable ion transport. As demonstrated by the FTIR spectra in Figure S7 (Supporting Information), the incorporation of the aerogel into the polymer electrolyte increased the dissociation ratio of LiTFSI from ≈84.7% to 94.4%.

Some potential inorganic or polymeric mechanical reinforcements were investigated, with improvements proven.[9,10,38,39] Compared to the previous developments, $SiO_2$ aerogel indeed has many unique properties. Its high porosity, ultrasmall pore size, large surface area, and favorable surface chemistry all play important roles in improving the overall performance of the composite electrolyte.

The flammability of the $SiO_2$-aerogel-reinforced CPE was evaluated using the flammability tests (Movie S1 and Figure S8, Supporting Information). In contrast to conventional carbonate- and ether-based liquid electrolytes, which can be easily ignited by an external flame source, the $SiO_2$-aerogel-reinforced CPE had low flammability and continued to exhibit good structural stability even after multiple exposures to an intense flame source. The low flammability offers the opportunity for safe batteries with high energy density.

A crosslinked-PEO electrolyte with the addition of SCN was used in our study because of its high ionic conductivity and relatively high melting point. It was reported that the addition of SCN can boost ionic conductivity by at least 1–2 orders of magnitude (Figure S9, Supporting Information),[40] but a major drawback is that it also significantly decreases the mechanical properties, rendering a weaker electrolyte vulnerable to uneven Li deposition. However, since the mechanical properties of

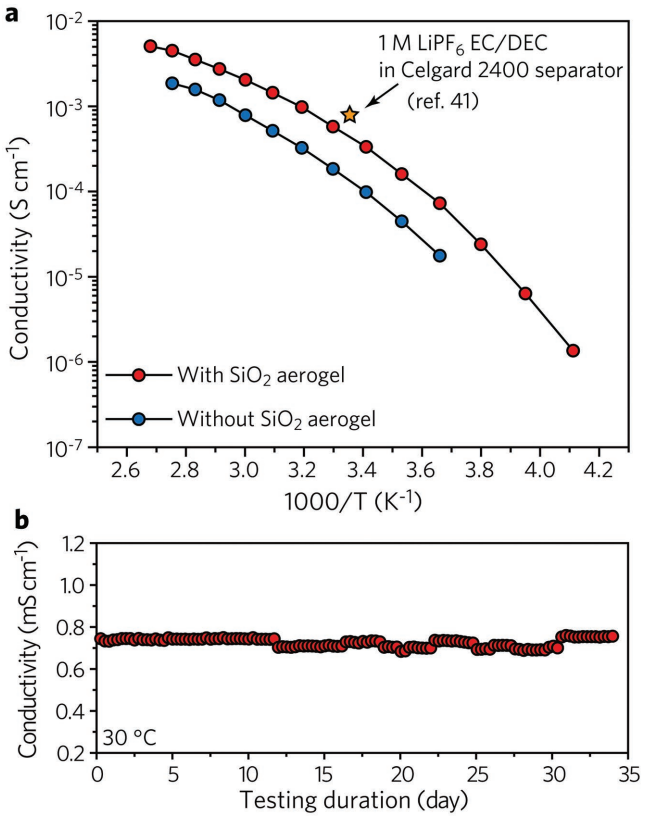


**Figure 2.** Characterizations of ionic conductivity. a) Arrhenius plots showing the temperature-dependent ionic conductivity of the electrolyte with and without $SiO_2$ aerogel film as the framework. The introduction of $SiO_2$ aerogel offers an approximately threefold improvement in ionic conductivity. The ambient value is close to that of 1 M $LiPF_6$ ethylene carbonate (EC)/diethyl carbonate (DEC) soaked in Celgard 2400 separator. b) Stability test of the ionic conductivity of a $SiO_2$-aerogel-reinforced CPE at 30 °C through an over 1 month of testing duration.

the composite electrolyte are dominated by the $SiO_2$ aerogel backbone as discussed later, any polymer electrolyte can be employed regardless of its mechanical properties. Furthermore, in contrast to conventional liquid plasticizers, SCN remains in the solid phase up to 57 °C, not much lower than that of PEO. As a consequence, the overall electrolyte remains solid for most anticipated battery operation conditions.

**Figure 2**a shows the ionic conductivity comparison between the electrolyte with (red) and without (blue) the incorporation of $SiO_2$ aerogel. The electrolyte films employed in the measurements were ≈600 µm in thickness. It was found that the crosslinked-PEO electrolyte with SCN already affords a relatively of ≈0.2 mS $cm^{-1}$ at 30 °C, outperforming most SPEs.[29] After the incorporation of the $SiO_2$ aerogel, a threefold enhancement in ionic conductivity was observed, achieving ≈0.6 mS $cm^{-1}$ at 30 °C. Considering that the crosslinked-PEO/SCN electrolyte already has a high ionic conductivity, a threefold enhancement beyond that is significant. At 40 °C, the CPE exhibited an ionic conductivity over 1.0 mS $cm^{-1}$, a value very close to that of liquid electrolytes with separator at room temperature (≈1 mS $cm^{-1}$ at 25 °C).[41,42] It is also noteworthy that even at a low temperature of 0 °C, a value of ≈0.1 mS $cm^{-1}$ was still retained. The enhanced ionic conductivity can be attributed to three effects. First, the nonconductive but highly porous $SiO_2$ aerogel occupies a minimal volume of the composite, maximizing the Li-ion conducting phase. Second, the ultrasmall, well-distributed, and interconnected domains of $SiO_2$ with acidic −OH surface maximize the Lewis acid–base interaction with anions, increasing the Li salt dissociation (Figure S6, Supporting Information) and thus forming a continuous highly conductive pathway through the whole electrolyte film. Third, the −C≡N in SCN can also potentially interact with −OH on $SiO_2$, which can help the dissociation of nitrile–$Li^+$ interaction and release more $Li^+$ carriers.[43]

The electrochemical stability window was determined by cyclic voltammetry from −0.15 to 5.0 V (Figure S11, Supporting Information) at 50 °C. It was found that the CPE is stable up to ≈4.4 V even at elevated temperature, guaranteeing stable cycling of typical commercial cathode materials such as LFP and $LiCoO_2$. Some minimal signals were observed in the range of 0–4.4 V, which are commonly observed in polymer electrolyte systems due to the reactions of the anions, the dissolution of Li in the electrode support, or the reaction of impurities.[44] Notably, no sign of the redox of SCN was observed in the scan, which excludes the potential hazards of cyanides formation in practical applications. The transference number of the $SiO_2$-aerogel-reinforced CPE was determined to be ≈0.38 (Figure S12, Supporting Information). In addition, a time-dependent impedance measurement was carried out at a fixed temperature of 30 °C (Figure 2b) to determine the electrochemical stability of the $SiO_2$-aerogel-reinforced CPE over time. Stable ionic conductivity without observable decay was obtained for over 1 month.

The elastic modulus obtained from nanoindentation of the crosslinked PEO with SCN, crosslinked PEO with both SCN and LiTFSI, crosslinked PEO with LiTFSI, $SiO_2$ aerogel, $SiO_2$ aerogel/PEO composite, and $SiO_2$ aerogel/PEO composite with LiTFSI (or $SiO_2$-aerogel-reinforced CPE) are shown in **Figure 3**a. In the nanoindentation test, an indenter was compressed into a material that can mimic the situation when Li dendrites start to evolve and interact with the electrolyte. The reported moduli include the uncertainties related to surface roughness and densification of the material under the indenter tip. Microtension tests were therefore performed to confirm that the modulus corresponded to the plateau of the nanoindentation modulus versus depth curves (see Figure S13 in the Supporting Information for modulus vs depth plots).

As expected and shown in Figure 3a, the modulus of the crosslinked PEO with SCN was relatively low (0.017 ± 0.0004 GPa), and the addition of LiTFSI gives a similar value, indicating a minimal effect of LiTFSI on the modulus in this polymer. The value is consistent with previously reported crosslinked-PEO/SCN electrolyte,[40] which is insufficient to effectively suppress Li dendrites. The modulus of the crosslinked PEO with LiTFSI (without SCN) was slightly higher (0.033 ± 0.0004 GPa). In contrast, the modulus of the $SiO_2$ aerogel alone was markedly higher at 0.21 ± 0.01 GPa. The measured modulus of the $SiO_2$ aerogel was checked against values predicted using cellular-solid mechanics (see the Supporting Information) and showed good agreement. The composite modulus was 0.29 ± 0.03 GPa (without LiTFSI) and 0.43 ± 0.01 GPa (with LiTFSI).

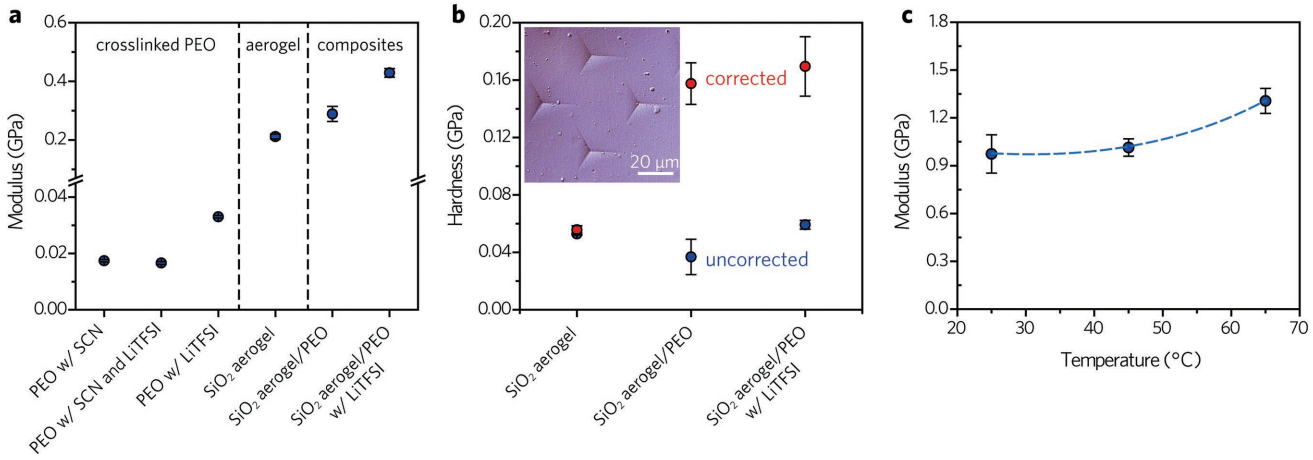


**Figure 3.** Thermomechanical characterizations. a) Elastic modulus of the crosslinked PEO with SCN, crosslinked PEO with both SCN and LiTFSi, crosslinked PEO with LiTFSI, $SiO_2$ aerogel, $SiO_2$-aerogel/PEO composite, and $SiO_2$-aerogel/PEO composite with LiTFSI (i.e., $SiO_2$-aerogel-reinforced CPE). b) The "uncorrected" (blue) and "corrected" (red) hardness of the $SiO_2$ aerogel, $SiO_2$-aerogel/PEO composite, and CPE. The inset shows a cross-polarized microscopic image of the residual indents on a composite specimen. c) Modulus of the $SiO_2$-aerogel/PEO composite as a function of temperature.

Clearly, the incorporation of the aerogel into the crosslinked PEO increased the modulus by more than tenfold, from 0.017 to 0.29 GPa, because the modulus of the composites was dominated by that of the $SiO_2$ aerogel.

The hardness of the $SiO_2$ aerogel and the composites are shown in Figure 3b. Hardness is a measure of the resistance against plastic deformation in a material. It characterizes the electrolyte resistance against permanent damages that may be caused by the growth of lithium dendrites. Hardness was calculated using $H = P/A_C$, where $P$ was the load and $A_C$ the contact area (see Figure S15 in the Supporting Information for load vs depth plots). It was observed that for the composites, the contact area detected by the nanoindenter was different from the area of the residual indents that remained on the specimen after testing. As a result, a manual calculation of the residual indent area was necessary to obtain the correct value for hardness.[45] Cross-polarized microscopy images (inset of Figure 3b and Figure S16 (Supporting Information)) and imaging software (ImageJ) were used to calculate the residual indent area. Two sets of hardness data are then reported, the "uncorrected" hardness that was determined based on the contact area detected by the nanoindenter ($SiO_2$ aerogel 53 ± 1 MPa, $SiO_2$ aerogel/PEO composite 37 ± 12 MPa, and CPE 59 ± 3 MPa), and the "corrected" hardness that was calculated based on the residual indent area and maximum load ($SiO_2$ aerogel 56 ± 3 MPa, $SiO_2$ aerogel/PEO composite 158 ± 14 MPa, and CPE 170 ± 21 MPa). Note that no hardness data are reported for the PEO specimens because no residual indents were observed during testing (Figure S17, Supporting Information), indicating full viscoelastic recovery.

The reason for the discrepancy between the detected area and the residual area for the composites is that there was an ≈2–4 μm PEO overburden on top of the aerogel. The PEO was able to viscoelastically deform without any evidence of residual deformation as noted above. As a result, no residual indentation was observed until the indenter reached the aerogel region. This means that the residual indent area, i.e., the area that deformed plastically and permanently, was smaller than the area detected by the nanoindenter. On the other hand, the uncorrected and corrected hardness of the $SiO_2$ aerogel agreed well with each other because it deformed irreversibly, clearly indicating the significant effect of the polymer on promoting "hardness" of the composites.

For cellular materials like the aerogel used in this study, the hardness can be related to the yield strength, $\sigma_{YS}$, using $H = R\sigma_{YS}$, where $R$ is a function of Poisson's ratio.[46] We note that for the ≈0.32 g cm$^{-3}$ low density brittle $SiO_2$ aerogel, its yield strength is its brittle crushing strength, $\sigma_f$.[47] Using a Poisson's ratio of 0.2 for the $SiO_2$ aerogel[48] and assuming a Poisson's ratio of 0.3 for the composites, $R$ was determined to be 2.6 and 2.8, respectively,[46] and resulting $\sigma_f$ values are shown in **Table 1**. The brittle crushing strength of the $SiO_2$ aerogel showed good agreement with values predicted using cellular-solid mechanics (see the Supporting Information). The brittle crushing strength of the composites were higher than that of the $SiO_2$ aerogel alone as the PEO supported the $SiO_2$ "cellular

**Table 1.** Corrected hardness, $R$, and calculated brittle crushing strength for $SiO_2$ aerogel and composites.

| | $SiO_2$ aerogel | $SiO_2$ aerogel/PEO composite (w/o LiTFSI) | $SiO_2$ aerogel/PEO composite (w/ LiTFSI) |
|---|---|---|---|
| Corrected hardness $H_{corr}$ [MPa] | 56 ± 3 | 158 ± 14 | 170 ± 21 |
| $R$[46] | 2.6 | 2.8 | 2.8 |
| Brittle crushing strength, $\sigma_f = \frac{H_{corr}}{R}$ [MPa] | 22 ± 1 | 56 ± 5 | 61 ± 8 |

frame" against bending and collapsing of the cell walls, and increased the strength of the composites.[49] The strength of the aerogel clearly had a marked effect on the strength of the PEO, and filling the aerogel with polymer increased the strength further.

The effect of temperature on the mechanical properties of $SiO_2$-aerogel/PEO composite is shown in Figure 3c. It was observed that the modulus increased slightly with increasing temperature. The ability of the composite to maintain its mechanical stiffness at elevated temperatures is important, making it a superior material over traditional polymer electrolytes whose mechanical stiffness degrades at elevated temperatures.[24,50,51]

To evaluate the cycling stability with the $SiO_2$-aerogel-reinforced CPE as the electrolyte, symmetric cells with Li foils as both electrodes were assembled and tested. Electrolytes that were ≈150 µm thick were employed in all the electrochemical tests conducted at ambient temperature (≈18 °C). As shown in **Figure 4**a, where stripping/plating cycles were carried out at a fixed current density of 0.05 mA $cm^{-2}$, a much more stable cycling for at least 450 cycles without internal short circuit was achieved for the electrolyte with $SiO_2$ aerogel. In contrast, the crosslinked-PEO electrolyte without $SiO_2$ aerogel exhibited a hard short circuit within tens of cycles due to the mechanical failure of the relatively weak electrolyte. The remarkable difference in cycle life strongly supports the effectiveness of the $SiO_2$-aerogel-reinforced CPE in dendrite suppression. The mechanical stability was further demonstrated with in situ optical cells (Figure S18, Supporting Information), where Li was continuously deposited to one electrode. Dendrite-induced short circuit can be observed in electrolyte without $SiO_2$ aerogel, while the aerogel-reinforced counterpart exhibited pronounced dendrite suppression effect. The polarization of the Li foil electrodes was further reduced with the incorporated $SiO_2$ aerogel (Figure 4a), which we attributed to the highly enhanced ionic conductivity by the interconnected mesoporous $SiO_2$ network. In addition, it is noted that the polarization observed in Figure 4a is composed of two

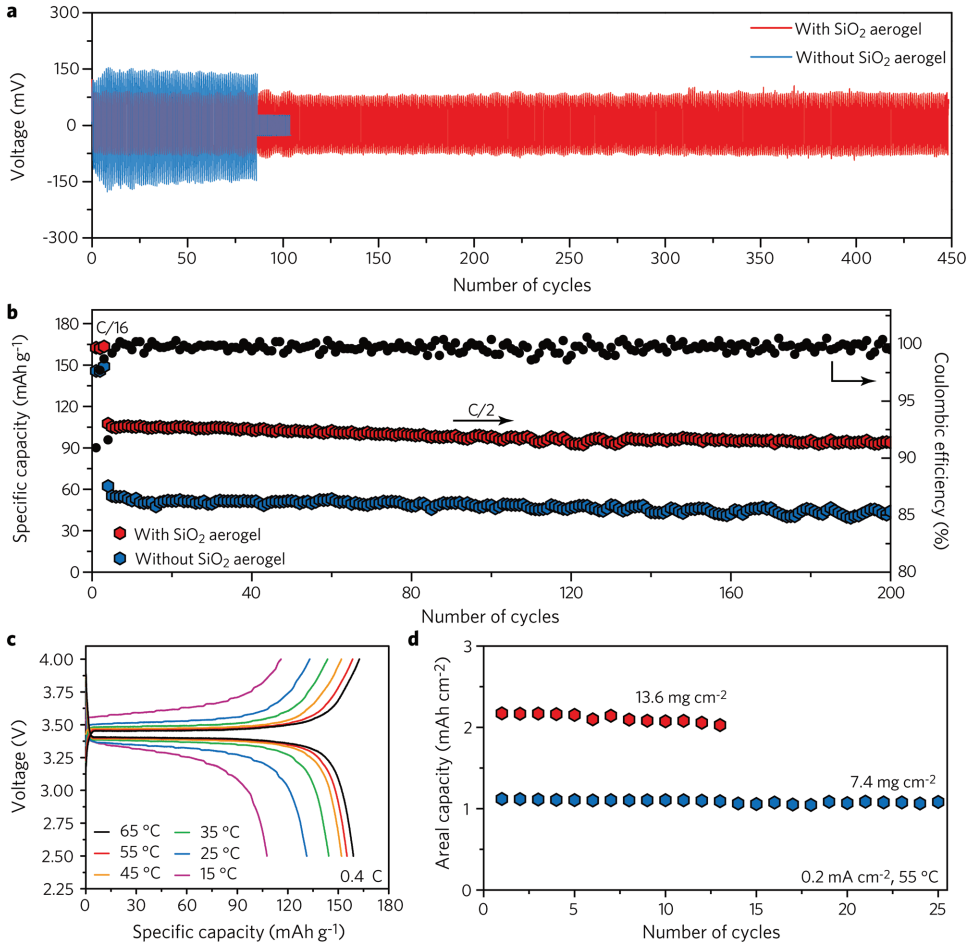


**Figure 4.** Symmetric and full-cell cycling with $SiO_2$-aerogel-reinforced CPE. a) Symmetric-cell cycling with a $SiO_2$-aerogel-reinforced CPE (red) and an electrolyte without $SiO_2$ aerogel (blue). The current density was fixed at 0.05 mA $cm^{-2}$ (with areal capacity of 0.05 mAh $cm^{-2}$) during the tests. The $SiO_2$-aerogel-reinforced CPE exhibits much longer cycle life without short circuit. b) Cycling stability (left *y*-axis) of LFP–Li cells with (red) and without (blue) $SiO_2$ aerogel framework at room temperature (≈18 °C), which exhibits stable cycling for at least 200 cycles. Three activation cycles were performed at C/16, followed by galvanostatic cycling at C/2 in the later cycles. The Coulombic efficiency of that with $SiO_2$ aerogel (red) is shown in the right *y*-axis. c) Voltage profiles of the LFP–Li cells at various temperatures from 15 to 65 °C, where the rate was fixed at 0.4 C. d) LFP–Li cells discharging cycling curves with high areal mass loading of 7.4 and 13.6 mg $cm^{-2}$. A current density of 0.2 mA $cm^{-2}$ was applied and the tests were performed at 55 °C.

components, namely, intrinsic overpotential and concentration potential (Figure S19, Supporting Information). The latter component originates from the formation of concentration gradient across the electrolyte, which would relax upon rest.

The electrochemical performance of the $SiO_2$-aerogel-reinforced CPE was then examined in a full-cell environment, where LFP–Li system was employed for the test. Figure 4b first shows the cycling stability of a LFP–Li cell with $SiO_2$-aerogel-reinforced CPE as the electrolyte, where stable cycling for at least 200 cycles with high capacity retention was obtained, outperforming that without $SiO_2$ aerogel. The good cyclability indicates the good electrochemical stability of the CPE within the full-cell environment. It is noted that the Coulombic efficiency (CE) of the cell slightly fluctuated, where some of the cycles exhibited >100% CE. This can be rationalized by the recovery of the temporary capacity loss in earlier cycles due to the possible disconnection at electrode-electrolyte interface (Figure S21, Supporting Information). Figure S22 (Supporting Information) compares the rate capability of the LFP–Li cells with $SiO_2$-aerogel-reinforced CPE and crosslinked-PEO electrolyte without aerogel, and Figure S23 (Supporting Information) shows the voltage profiles at different rates. Notably improved capacity retention was observed at various rate from C/16 to C/2. Especially at C/2, an ≈3 times higher capacity was retained. Furthermore, a temperature-dependent galvanostatic cycling was conducted from 15 to 65 °C at a constant rate of 0.4 C, with the corresponding voltage profiles at various temperatures presented in Figure 4c. It is noted that even at a low temperature of 15 °C, a relatively high capacity of ≈105 mAh $g^{-1}$ was retained. Once the temperature is elevated slightly to 35 °C, a much higher specific capacity of ≈145 mAh $g^{-1}$ with low polarization (≈134 mV, Figure S24, Supporting Information) was achieved. An increase in temperature from 45 to 65 °C further boosted the capacity to near theoretical values (theoretical: 170 mAh $g^{-1}$).

Furthermore, we demonstrated LFP–Li all-solid-state batteries with high cathode mass loading of 7.4 and 13.6 mg $cm^{-2}$ using the $SiO_2$-aerogel-reinforced CPE (Figure 4d and Figure S25 (Supporting Information)), where layered Li–reduced graphene oxide (rGO) composite electrodes[5] with limited areal Li capacity of ≈6 mAh $cm^{-2}$ was employed as the anode. The employment of Li–ethylene carbonate (EC)/diethyl carbonate (DEC) composite can effectively reduce the volume change and guarantee good interfacial contact. High areal capacity of ≈1.1 and ≈2.1 mAh $cm^{-2}$ were obtained, demonstrating the feasibility of all-solid full cell operation with practical areal capacity. The overall outstanding electrochemical performance shed light on the all-solid-state Li batteries that can operate efficiently and safely.

In all, we designed a new class of composite electrolyte composed of an interconnected $SiO_2$ aerogel backbone and a highly conductive crosslinked-PEO-based electrolyte. The formation of composite gives rise to much higher modulus and higher ionic conductivity than those reported before (Table S1, Supporting Information). The design methodology and the corresponding material properties in this contribution are distinct from the conventional composite electrolytes fabricated by mechanical blending of ceramic filler powders, polymers, and Li salts (Figure S26, Supporting Information). The preformation of the continuous $SiO_2$ aerogel network plays a key role, and has been demonstrated to resolve major problems, including mediocre mechanical properties and ionic conductivity, as well as powder agglomeration, in the mechanical blend counterparts. The introduction of the $SiO_2$ aerogel offers at least three merits. First, with the strong interconnected $SiO_2$ aerogel backbone, the mechanical properties of the composite were less dependent on the mechanically weak polymer, and had at least ≈1 order of magnitude higher elastic modulus compared with conventional polymer electrolytes. Second, the large-surface, uniformly distributed, and ultrasmall $SiO_2$ domains, and favorable acidic surface maximize their interaction with anions of the Li salt and form continuous pathways within the composite, which further contributes to the higher level of salt dissociation and enhanced ionic conductivity. Third, the $SiO_2$-aerogel/PEO composite was able to maintain its mechanical stiffness at elevated temperatures, in contrast to conventional polymer electrolytes whose stiffness degrade significantly at those temperatures. As a consequence of these merits, a threefold enhancement in ionic conductivity was obtained, reaching ≈0.6 mS $cm^{-1}$ at 30 °C. The mechanical properties of the composite electrolytes demonstrated an elastic modulus of ≈0.43 GPa, at least 1 order of magnitude higher than that of the crosslinked PEO-based electrolyte, and a markedly enhanced hardness of ≈170 MPa. As a result, notable dendrite suppression effect was obtained without internal short circuit at prolonged cycles. Finally, full cells with LFP as the cathodes were examined and exhibited stable cycling and good rate capability at ambient temperature (≈18 °C). Even at a low temperature of 15 °C, high capacity of ≈105 mAh $g^{-1}$ was still retained at 0.4 C. LFP–Li full cells with high areal capacity up to 2.1 mAh $cm^{-2}$ was also achieved. The $SiO_2$-aerogel-reinforced CPE not only proves a promising design principle on strong and highly Li-ion conductive polymer electrolytes, but also paves the way for the next-generation high-energy all-solid-state Li batteries and their safe operation.

## Supporting Information

Supporting Information is available from the Wiley Online Library or from the author.

## Acknowledgements

D.L. and P.Y.Y. contributed equally to this work. Y.C. acknowledges the support from the Assistant Secretary for Energy Efficiency and Renewable Energy, Office of Vehicle Technologies of the U.S. Department of Energy under the Battery Materials Research (BMR) program and Battery500 consortium. Part of this work was performed at the Stanford Nano Shared Facilities (SNSF), supported by the National Science Foundation under Award No. ECCS-1542152.

## Conflict of Interest

The authors declare no conflict of interest.

## Keywords

composite polymer electrolytes, $SiO_2$ aerogels, solid-state batteries

Received: April 26, 2018
Revised: May 21, 2018
Published online:

 

[1] M. Armand, J. M. Tarascon, *Nature* **2008**, *451*, 652.
[2] J. B. Goodenough, K.-S. Park, *J. Am. Chem. Soc.* **2013**, *135*, 1167.
[3] D. Lin, Y. Liu, Y. Cui, *Nat. Nanotechnol.* **2017**, *12*, 194.
[4] W. Xu, J. Wang, F. Ding, X. Chen, E. Nasybulin, Y. Zhang, J.-G. Zhang, *Energy Environ. Sci.* **2014**, *7*, 513.
[5] D. Lin, Y. Liu, Z. Liang, H.-W. Lee, J. Sun, H. Wang, K. Yan, J. Xie, Y. Cui, *Nat. Nanotechnol.* **2016**, *11*, 626.
[6] H. J. Peng, J. Q. Huang, X. B. Cheng, Q. Zhang, *Adv. Energy Mater.* **2017**, *7*, 1700260.
[7] Y. Liu, D. Lin, Z. Liang, J. Zhao, K. Yan, Y. Cui, *Nat. Commun.* **2016**, *7*, 10992.
[8] D. Aurbach, *J. Power Sources* **2000**, *89*, 206.
[9] Z. Tu, Y. Kambe, Y. Lu, L. A. Archer, *Adv. Energy Mater.* **2014**, *4*, 1300654.
[10] Z. Tu, M. J. Zachman, S. Choudhury, S. Wei, L. Ma, Y. Yang, L. F. Kourkoutis, L. A. Archer, *Adv. Energy Mater.* **2017**, *7*, 1602367.
[11] K. Xu, *Chem. Rev.* **2004**, *104*, 4303.
[12] R. Kanno, M. Murayama, *J. Electrochem. Soc.* **2001**, *148*, A742.
[13] A. Hayashi, S. Hama, H. Morimoto, M. Tatsumisago, T. Minami, *J. Am. Ceram. Soc.* **2001**, *84*, 477.
[14] N. Kamaya, K. Homma, Y. Yamakawa, M. Hirayama, R. Kanno, M. Yonemura, T. Kamiyama, Y. Kato, S. Hama, K. Kawamoto, *Nat. Mater.* **2011**, *10*, 682.
[15] Y. Inaguma, C. Liquan, M. Itoh, T. Nakamura, T. Uchida, H. Ikuta, M. Wakihara, *Solid State Commun.* **1993**, *86*, 689.
[16] R. Murugan, V. Thangadurai, W. Weppner, *Angew. Chem., Int. Ed.* **2007**, *46*, 7778.
[17] V. Thangadurai, S. Narayanan, D. Pinzaru, *Chem. Soc. Rev.* **2014**, *43*, 4714.
[18] U. v. Alpen, A. Rabenau, G. Talat, *Appl. Phys. Lett.* **1977**, *30*, 621.
[19] H. Aono, E. Sugimoto, Y. Sadaoka, N. Imanaka, G. y. Adachi, *J. Electrochem. Soc.* **1990**, *137*, 1023.
[20] J. Bates, N. Dudney, G. Gruzalski, R. Zuhr, A. Choudhury, C. Luck, J. Robertson, *Solid State Ionics* **1992**, *53*, 647.
[21] F. Croce, G. Appetecchi, L. Persi, B. Scrosati, *Nature* **1998**, *394*, 456.
[22] G. Stone, S. Mullin, A. Teran, D. Hallinan, A. Minor, A. Hexemer, N. Balsara, *J. Electrochem. Soc.* **2012**, *159*, A222.
[23] D. Lin, W. Liu, Y. Liu, H. R. Lee, P.-C. Hsu, K. Liu, Y. Cui, *Nano Lett.* **2015**, *16*, 459.
[24] W. H. Meyer, *Adv. Mater.* **1998**, *10*, 439.
[25] R. Bouchet, S. Maria, R. Meziane, A. Aboulaich, L. Lienafa, J.-P. Bonnet, T. N. Phan, D. Bertin, D. Gigmes, D. Devaux, R. Denoyel, M. Armand, *Nat. Mater.* **2013**, *12*, 452.
[26] Z. Deng, Z. Wang, I.-H. Chu, J. Luo, S. P. Ong, *J. Electrochem. Soc.* **2016**, *163*, A67.
[27] Y. Ren, Y. Shen, Y. Lin, C.-W. Nan, *Electrochem. Commun.* **2015**, *57*, 27.
[28] Y. Zhu, X. He, Y. Mo, *ACS Appl. Mater. Interfaces* **2015**, *7*, 23685.
[29] R. Agrawal, G. Pandey, *J. Phys. D: Appl. Phys.* **2008**, *41*, 223001.
[30] M. D. Tikekar, S. Choudhury, Z. Tu, L. A. Archer, *Nat. Energy* **2016**, *1*, 16114.
[31] A. Manuel Stephan, *Eur. Polym. J.* **2006**, *42*, 21.
[32] S. Choudhury, R. Mangal, A. Agrawal, L. A. Archer, *Nat. Commun.* **2015**, *6*, 10101.
[33] P.-J. Alarco, Y. Abu-Lebdeh, A. Abouimrane, M. Armand, *Nat. Mater.* **2004**, *3*, 476.
[34] K. K. Fu, Y. Gong, J. Dai, A. Gong, X. Han, Y. Yao, C. Wang, Y. Wang, Y. Chen, C. Yan, *Proc. Natl. Acad. Sci. USA* **2016**, *113*, 7094.
[35] N. B. Aetukuri, S. Kitajima, E. Jung, L. E. Thompson, K. Virwani, M. L. Reich, M. Kunze, M. Schneider, W. Schmidbauer, W. W. Wilcke, *Adv. Energy Mater.* **2015**, *5*, 1500265.
[36] A. S. Dorcheh, M. Abbasi, *J. Mater. Process. Technol.* **2008**, *199*, 10.
[37] A. C. Pierre, A. Rigacci, in *Aerogels Handbook*, (Eds: M. M. Koebel, N. Leventis), Springer, Berlin, Germany **2011**, pp. 21–45.
[38] J. Zhang, Y. Bai, X.-G. Sun, Y. Li, B. Guo, J. Chen, G. M. Veith, D. K. Hensley, M. P. Paranthaman, J. B. Goodenough, S. Dai, *Nano Lett.* **2015**, *15*, 3398.
[39] D. Li, L. Chen, T. Wang, L.-Z. Fan, *ACS Appl. Mater. Interfaces* **2018**, *10*, 7069.
[40] M. Echeverri, C. Hamad, T. Kyu, *Solid State Ionics* **2014**, *254*, 92.
[41] J. Song, Y. Wang, C. Wan, *J. Electrochem. Soc.* **2000**, *147*, 3219.
[42] S. S. Zhang, *J. Power Sources* **2007**, *164*, 351.
[43] Z. Wang, X. Huang, L. Chen, *Electrochem. Solid-State Lett.* **2003**, *6*, E40.
[44] F. Bonino, B. Scrosati, A. Selvaggi, *Solid State Ionics* **1986**, *18*, 1050.
[45] J. Hay, *Exp. Tech.* **2009**, *33*, 66.
[46] M. Shaw, T. Sata, *Int. J. Mech. Sci.* **1966**, *8*, 469.
[47] J. C. Wong, H. Kaymak, S. Brunner, M. M. Koebel, *Microporous Mesoporous Mater.* **2014**, *183*, 23.
[48] J. Gross, G. Reichenauer, J. Fricke, *J. Phys. D: Appl. Phys.* **1988**, *21*, 1447.
[49] Y. W. Kwon, R. E. Cooke, C. Park, *Mater. Sci. Eng., A* **2003**, *343*, 63.
[50] J. Wu, Y. S. Thio, F. S. Bates, *J. Polym. Sci., Part B: Polym. Phys.* **2005**, *43*, 1950.
[51] F. Alloin, A. D'Aprea, N. E. Kissi, A. Dufresne, F. Bossard, *Electrochim. Acta* **2010**, *55*, 5186.